Article

SOURCE DATA | TRANSPARENT PROCESS

THE EMBO JOURNAL

The ASC-1 complex promotes translation initiation by scanning ribosomes

Yuki Kito[1,†], Akinobu Matsumoto[1,*,†], Kazuya Ichihara[1,†], Chisa Shiraishi[1], Ronghao Tang[1], Atsushi Hatano[2], Masaki Matsumoto[2], Peixun Han[3,4], Shintaro Iwasaki[3,4] & Keiichi I Nakayama[1,**]

Abstract

Translation initiates when the eIF4F complex binds the 5′ mRNA cap, followed by 5′ untranslated region scanning for the start codon by scanning ribosomes. Here, we demonstrate that the ASC-1 complex (ASCC), which was previously shown to promote the dissociation of colliding 80S ribosomes, associates with scanning ribosomes to regulate translation initiation. Selective translation complex profiling (TCP-seq) analysis revealed that ASCC3, a helicase domain-containing subunit of ASCC, localizes predominantly to the 5′ untranslated region of mRNAs. Ribo-seq, TCP-seq, and luciferase reporter analyses showed that ASCC3 knockdown impairs 43S preinitiation complex loading and scanning dynamics, thereby reducing translation efficiency. Whereas eIF4A, an RNA helicase in the eIF4F complex, is important for global translation, ASCC was found to regulate the scanning process for a specific subset of transcripts. Our results have thus revealed that ASCC is required not only for dissociation of colliding 80S ribosomes but also for efficient translation initiation by scanning ribosomes at a subset of transcripts.

Keywords ASCC; eIF4A; scanning ribosome; Sel-TCP-MS; translation initiation
Subject Category Translation & Protein Quality
DOI 10.15252/embj.2022112869 | Received 19 October 2022 | Revised 18 March 2023 | Accepted 27 March 2023 | Published online 24 April 2023
The EMBO Journal (2023) 42: e112869

Introduction

Most translation of mRNAs in mammalian cells is initiated by binding of the eukaryotic initiation factor 4F (eIF4F) complex to the cap structure at the 5′ end of the mRNA followed by binding of the 43S preinitiation complex (PIC) to the eIF4F-mRNA complex (Hinnebusch, 2017; Shirokikh & Preiss, 2018; Bohlen *et al*, 2020; Wagner *et al*, 2020). Generation of the 43S PIC is mediated by the initial formation of a ternary complex by eIF2, GTP, and Met-tRNA$_i$ and the subsequent binding of this complex to the 40S ribosomal subunit together with the eIF3 complex (consisting of 13 subunits: eIF3A to eIF3M), eIF1, eIF1A, and eIF5. The eIF4F complex consists of the scaffolding protein eIF4G, the cap-binding protein eIF4E, and the DEAD-box helicase eIF4A. After eIF4F binds to the cap structure, eIF4G interacts with eIF3 and thereby facilitates recruitment of the 43S PIC to the mRNA, resulting in the formation of the 48S complex (scanning ribosome; LeFebvre *et al*, 2006; Villa *et al*, 2013; Kumar *et al*, 2016; Querido *et al*, 2020). Following recognition of the initiation codon by the scanning ribosome, eIF5B mediates binding to the 60S ribosomal subunit and consequent formation of the 80S ribosome for translational elongation (Lapointe *et al*, 2022).

Several RNA helicases play a major role in translation initiation (Shen & Pelletier, 2020). All RNA helicases are classified into six superfamilies (SFs), with the eukaryotic enzymes belonging to SF1 or SF2. SF2 comprises subfamilies such as DExD-box (DDX), DExH-box (DHX), and Ski2-like (Singleton *et al*, 2007; Jankowsky, 2011). eIF4A is a DDX RNA helicase, with three paralogs of this protein having been identified in mammals: eIF4A1 (DDX2A), eIF4A2 (DDX2B), and eIF4A3 (DDX48). eIF4A1 and eIF4A2 function in translation initiation, whereas eIF4A3 is a component of the exon junction complex (Chan *et al*, 2004). In addition to eIF4A, other DDX and DHX helicases also contribute to translation initiation (Shen & Pelletier, 2020). DDX3 binds to helix 16 of rRNA of the scanning ribosome, which is located in the immediate vicinity of the mRNA entry channel, and it promotes translation initiation of transcripts with a structured 5′ untranslated region (5′-UTR; Calviello *et al*, 2021). DHX9 and DHX36 facilitate translation initiation by unwinding the G-quadruplex structures of the 5′-UTR (Murat *et al*, 2018).

In the absence of a stop codon, or in the case of premature polyadenylation of mRNA, translation of the poly(A) sequence leads to the generation of basic polylysine peptides followed by translation arrest and rapid degradation of the nascent peptides by the ribosome-associated quality control (RQC) pathway (Bengtson & Joazeiro, 2010; Brandman *et al*, 2012; Joazeiro, 2019; Ikeuchi *et al*, 2019a). Collision of the stalled ribosome with a following

1 Division of Cell Biology, Medical Institute of Bioregulation, Kyushu University, Fukuoka, Japan
2 Department of Omics and Systems Biology, Graduate School of Medical and Dental Sciences, Niigata University, Niigata, Japan
3 RNA Systems Biochemistry Laboratory, RIKEN Cluster for Pioneering Research, Wako, Japan
4 Department of Computational Biology and Medical Sciences, Graduate School of Frontier Sciences, The University of Tokyo, Kashiwa, Japan
*Corresponding author. Tel: +81926426816; E-mail: akinobu@bioreg.kyushu-u.ac.jp
**Corresponding author. Tel: +81926426815; E-mail: nakayak1@bioreg.kyushu-u.ac.jp
†These authors contributed equally to this work

ribosome results in the formation of a di-ribosome (disome), which is directly recognized by the ubiquitin ligase ZNF598 in mammals (Hel2 in yeast). This enzyme catalyzes the formation of K63-linked ubiquitin chains on mammalian eS10 (uS10 in yeast), a subunit of the 40S ribosome (Ikeuchi *et al*, 2019b). The ubiquitylated disome is dissociated by the RQC-trigger (RQT) complex. The RQT complex was first identified in yeast as a complex consisting of the RNA helicase Slh1 (Rqt2), Cue3 (Rqt3), and Ykr023w (Rqt4). In mammals, the ASC-1 complex (ASCC) consists of four subunits—ASC1 (also known as TRIP4), ASCC1, ASCC2, and ASCC3—and three of these four subunits (ASC1, ASCC2, and ASCC3) are homologous to those of the yeast RQT complex. ASCC disassembles the leading ribosome of disomes in an ATP-dependent manner in both a mammalian cell-free system and mammalian cells (Hashimoto *et al*, 2020; Juszkiewicz *et al*, 2020).

We here combined the scanning ribosome purification method used in selective translation complex profile sequencing (Sel-TCP-seq) with mass spectrometry (Sel-TCP-MS) to comprehensively identify components of eIF4A-bound scanning ribosomes (Ichihara *et al*, 2021; Bohlen *et al*, 2023) and found that ASCC associates with the scanning ribosomes. Sel-TCP-seq analysis revealed that ASCC3 localized predominantly to the 5′-UTR of mRNAs, and depletion of ASCC3 resulted in altered scanning and translation efficiencies for a subset of transcripts. Our results thus uncover a previously unknown function of ASCC in the regulation of translation initiation that is mediated by binding to scanning ribosomes.

Results

Sel-TCP-MS analysis of eIF4A1-bound scanning ribosomes

Ribosome profiling (also known as Ribo-seq) visualizes the elongation step of 80S ribosomes, but it is unable to monitor the dynamics of scanning ribosomes (Ingolia *et al*, 2009). TCP-seq was developed to overcome this limitation by capturing the positions of all types of ribosome-mRNA complex throughout the transcriptome (Archer *et al*, 2016; Shirokikh *et al*, 2017). Given that the interaction between scanning ribosomes and mRNAs is weak, TCP-seq requires formalin fixation of translation complexes in living cells. Translation intermediates are then footprinted with RNase, and small ribosomal subunit (SSU) and 80S ribosome (RS) fractions are separated by sucrose density gradient centrifugation for deep sequencing. In addition, Sel-TCP-seq, which combines TCP-seq with immunopurification of ribosomes associated with a factor of interest, reveals the dynamics of translation factors (Bohlen *et al*, 2020; Wagner *et al*, 2020).

To identify more comprehensively components of scanning ribosomes, we purified eIF4A1-bound scanning ribosomes from the SSU fraction of HEK293T cells stably expressing eIF4A1 with an NH_2-terminal 3 × FLAG tag (eIF4A1-FLAG OE) on the basis of the Sel-TCP-seq method so as to deplete other macromolecular complexes present in the SSU fraction (Fig 1A and B). Immunoprecipitates prepared from the SSU fraction with antibodies to FLAG were subjected to semiquantitative liquid chromatography and tandem MS (LC–MS/MS) analysis. A total of 1,690 proteins were identified as components of the eIF4A1-bound scanning ribosomes in that they were commonly detected in three replicates of eIF4A1-bound scanning ribosome samples, with iBAQ (intensity-based absolute quantification) values > 10 times as great as those for the control sample in each replicate (Fig 1C, Dataset EV1). To investigate the possibility of nonspecific binding, we searched CRAPome (contaminant repository for affinity purification–mass spectrometry data, https://reprint-apms.org) and found that 178 of the 1,690 proteins were included in the repository. We therefore assumed that the 1,512 proteins that were identified in all three replicates and found to be CRAPome negative were components of the eIF4A1-bound scanning ribosomes (Fig 1C, Dataset EV1). Gene ontology (GO) term analysis for the proteins in the eIF4A1-bound scanning ribosomes revealed enrichment of several translation initiation–related terms, indicative of successful purification of scanning ribosomes (Fig 1D, Dataset EV2).

RNA helicases play a major role in translation initiation, and we found that many DDX and DHX helicases were present in the eIF4A1-bound scanning ribosomes (Fig 1E). Of note, ASCC3, a Ski2-like helicase known to contribute to the dissociation of colliding 80S ribosomes, was also detected in the eIF4A1-bound scanning ribosomes (Fig 1E). In addition, all other components of ASCC (ASC1, ASCC1, and ASCC2) were also identified (Fig 1E). These results indicated that ASCC binds not only to the 80S ribosome but also to the scanning ribosome.

ASCC binds to scanning ribosomes

We previously established HEK293T cells harboring the V5 tag sequence at the COOH terminus of endogenous eIF3D and the 3 × FLAG tag at the NH_2 terminus of endogenous eIF4E (eIF3D-V5/eIF4E-FLAG double knock-in (dKI); Ichihara *et al*, 2021). To confirm the association of ASCC with scanning ribosomes, we used these cells to purify eIF4E-bound scanning ribosomes and eIF3D-bound scanning ribosomes, and we found that ASCC3 was detected in both the eIF4E-bound and eIF3D-bound scanning ribosomes (Fig 2A, Appendix Table S1). Furthermore, we generated HEK293T cells in which the 3 × FLAG tag sequence was inserted at the NH_2 terminus of endogenous eIF4A1 or ASCC3 (eIF4A1-FLAG KI and ASCC3-FLAG KI, respectively) with the use of the CRISPR-Cas9 system (Appendix Fig S1A and B). Whereas ASCC1, ASCC2, and ASCC3 were associated with the eIF4A1-bound scanning ribosomes purified from eIF4A1-FLAG KI cells (Fig 2B, Appendix Table S1), virtually no eIF4F or eIF3 components were detected in immunoprecipitates purified from ASCC3-FLAG KI cells (Fig 2C, Appendix Table S1). However, the binding of ASCC3 to eIF4F and eIF3 was observed in immunoprecipitates purified from HEK293T cells stably expressing ASCC3 with an NH_2-terminal 3 × FLAG tag (ASCC3-FLAG OE; Fig 2D and E, Appendix Table S1). This difference suggested that, whereas many scanning ribosomes bind to ASCC3, only a small fraction of ASCC3 binds to scanning ribosomes, with most ASCC3 possibly binding to other macromolecular complexes. The differences in immunoprecipitation efficiency apparent for eIF3D-V5, eIF4E-FLAG, and eIF4A1-FLAG in these experiments (Appendix Table S1) may be attributable to the differences in antibodies used, in the steric positions of the epitope tags, or in both. Given that ASCC3 contributes to the disassembly of colliding 80S ribosomes, we also established HEK293T cells harboring the hemagglutinin (HA) tag sequence at the COOH terminus of endogenous RPL7A (RPL7A-HA KI; Appendix Fig S1C) and found that ASCC3 also bound to the 80S ribosome (Fig 2F, Appendix Table S1).

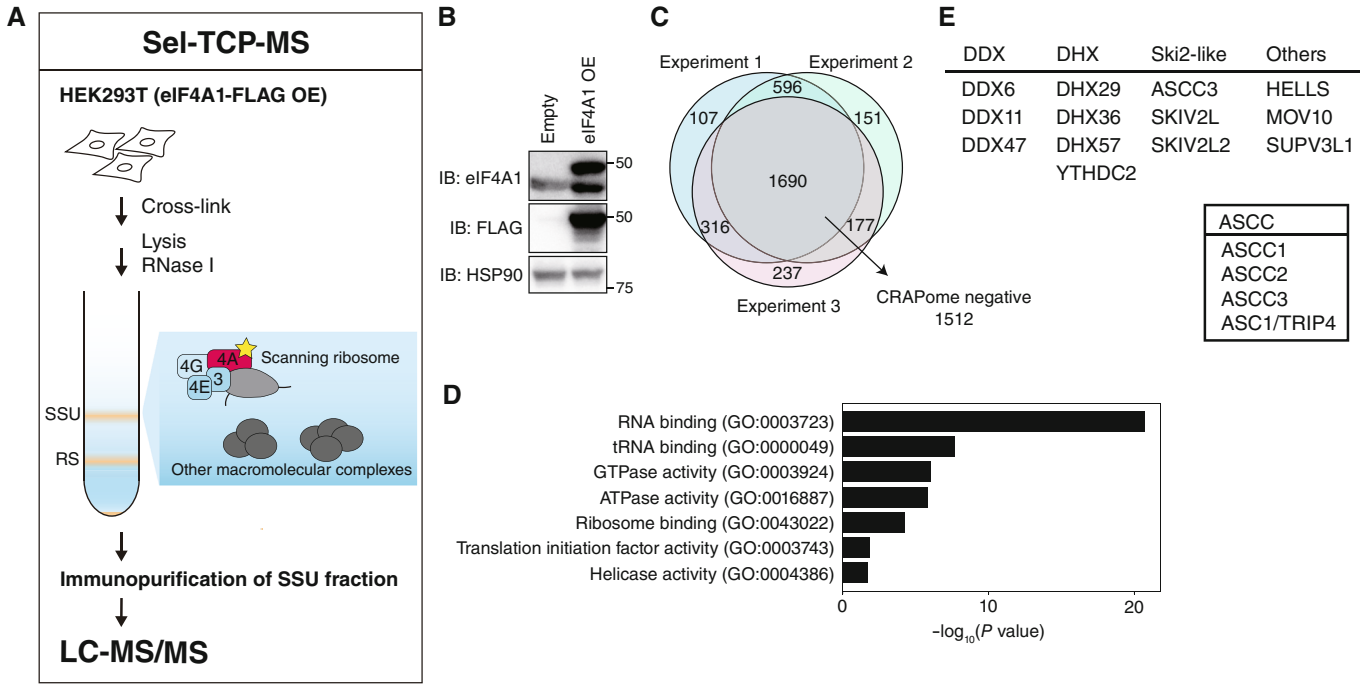

Figure 1. Sel-TCP-MS analysis of eIF4A1-bound scanning ribosomes in HEK293T cells.

A Schematic representation of the Sel-TCP-MS protocol for analysis of eIF4A1-bound scanning ribosomes.

B Immunoblot (IB) analysis of eIF4A1, FLAG, and HSP90 (loading control) in HEK293T cells either overexpressing (OE) eIF4A1 with an NH_2-terminal 3 × FLAG tag or infected with the corresponding empty lentivirus. Molecular sizes are indicated in kilodaltons.

C Venn diagram showing the numbers of identified proteins of eIF4A1-bound scanning ribosomes in three biological replicates of HEK293T cells stably expressing eIF4A1-FLAG.

D GO term analysis of identified proteins of eIF4A1-bound scanning ribosomes. Representative findings are presented.

E Lists of SF2 helicase proteins and ASCC subunits identified as components of eIF4A1-bound scanning ribosomes. SF2 helicase proteins are divided into DDX, DHX, Ski2-like, and other subfamilies, and ASCC is shown in a separate box.

Source data are available online for this figure.

Most, but not all, ASCC3 associates with the 5′-UTR of mRNAs

To visualize the dynamics of ASCC3-bound ribosomes, we performed Sel-TCP-seq analysis of ASCC3-FLAG with the use of SSU and RS fractions prepared from ASCC3-FLAG KI cells. In addition, we performed Sel-TCP-seq analysis of eIF4E-FLAG, eIF4A1-FLAG, and RPL7A-HA with eIF3D-V5/eIF4E-FLAG dKI, eIF4A1-FLAG KI, and RPL7A-HA KI cells (Dataset EV3). Metagene analysis with the full length of the resulting footprints showed that eIF4E-FLAG and eIF4A1-FLAG in the SSU fraction localized predominantly to the 5′-UTR of mRNAs, whereas the SSU input showed some 80S contamination (Figs 3A and EV1A). The RS input also showed some contamination with scanning ribosomes, and most footprints of eIF4E-FLAG and eIF4A1-FLAG purified from the RS fraction were localized to the 5′-UTR (Figs 3A and EV1A). Given that eIF4F and eIF3 were previously shown to bind to the 80S ribosome during translation of an upstream open reading frame (uORF; Bohlen *et al*, 2020), the RS footprints at the 5′-UTR may indicate translation of a uORF. Most footprints of RPL7A-HA purified from the RS fraction were localized to the coding sequence (CDS; Fig 3B).

Metagene analysis of ASCC3-FLAG revealed that footprints of scanning ribosomes in the 5′-UTR and those of 80S ribosomes in the CDS were apparent in both the SSU and RS fractions (Fig 3C). Footprints in the 5′-UTR were more abundant than those in the CDS region in both the SSU and RS fractions, indicating that ASCC preferentially associates with scanning ribosomes. The footprints of ASCC3-FLAG in the CDS region were more abundant than those of eIF4E-FLAG and eIF4A1-FLAG in the CDS region, consistent with the notion that ASCC also contributes to the disassembly of colliding 80S ribosomes (Hashimoto *et al*, 2020; Juszkiewicz *et al*, 2020). To assess further the enrichment of the various factors, we generated plots for the value of immunoprecipitate minus input. For the initiation factors eIF4E and eIF4A1, this value was > 0 in the 5′-UTR and negative in the CDS, and ASCC3 showed a similar pattern (Fig EV1B). For RPL7A, the value was > 0 but negligible in the CDS (Fig EV1B), suggesting that, for some unknown reason, the 80S ribosome was not well enriched.

We also performed metagene plot analysis using only the 5′ end of footprints, as done previously (Bohlen *et al*, 2020; Wagner *et al*, 2020), both with our data (eIF4E) and with those from these previous studies (eIF4E and eIF3B, respectively). We found that the length of SSU fragments and the extent of their accumulation around the start codon differed slightly among the three studies (Appendix Fig S2A). These differences are likely attributable to differences in cell type or TCP-seq protocols (see Discussion for more details). Metagene analysis with the 5′ end of the footprints for

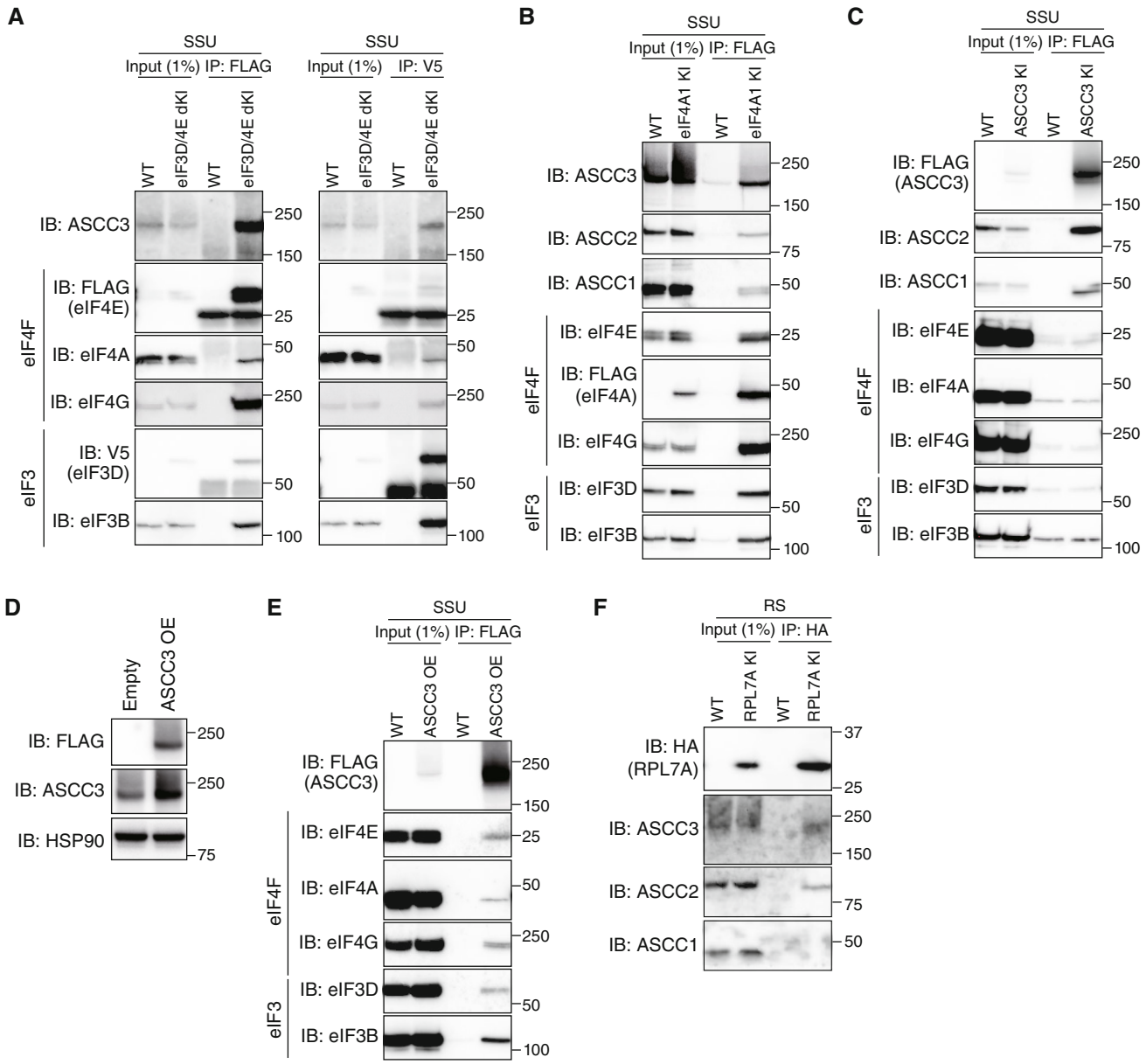

Figure 2. ASCC associates with scanning ribosomes.

A Immunoblot analysis with the indicated antibodies of immunoprecipitates (IP) prepared from the SSU fraction of eIF3D-V5/eIF4E-FLAG dKI HEK293T cells (eIF3D/4E dKI) or wild-type (WT) cells with antibodies to the epitope tags. The SSU fraction (input) was also analyzed directly. Cells were fixed with formalin, cell lysates were treated with RNase, and the SSU and RS fractions were separated by sucrose density gradient centrifugation before immunopurification. Molecular sizes are indicated in kilodaltons.

B, C Immunoblot analysis with the indicated antibodies of immunoprecipitates prepared as in A from the SSU fraction of eIF4A1-FLAG KI HEK293T cells (eIF4A1 KI) (B) or ASCC3-FLAG KI HEK293T cells (ASCC3 KI) (C).

D Immunoblot analysis of HEK293T cells either overexpressing (OE) ASCC3-FLAG or infected with the corresponding empty lentivirus.

E, F Immunoblot analysis with the indicated antibodies of immunoprecipitates prepared as in (A) from the SSU fraction of ASCC3-FLAG OE HEK293T cells (ASCC3 OE) (E) or from the RS fraction of RPL7A-HA KI HEK293T cells (RPL7A KI) (F).

Source data are available online for this figure.

eIF4E-FLAG purified from the SSU fraction in our study showed the 5′-UTR extension (tail) of the start footprints extending from 30 to 75 nucleotides (Appendix Fig S2A), which reflects the process by which the scanning ribosome initiates translation (Bohlen *et al*, 2020; Wagner *et al*, 2020). This tail was also observed in the Sel-TCP-seq data for eIF4A1-FLAG and ASCC3-FLAG (Appendix Fig S2B), further supporting the notion that ASCC3 binds to the scanning ribosome.

For eIF4E-FLAG, eIF4A1-FLAG, RPL7A-HA, and ASCC3-FLAG, the TPM (transcripts per kilobase million) values of Sel-TCP-seq

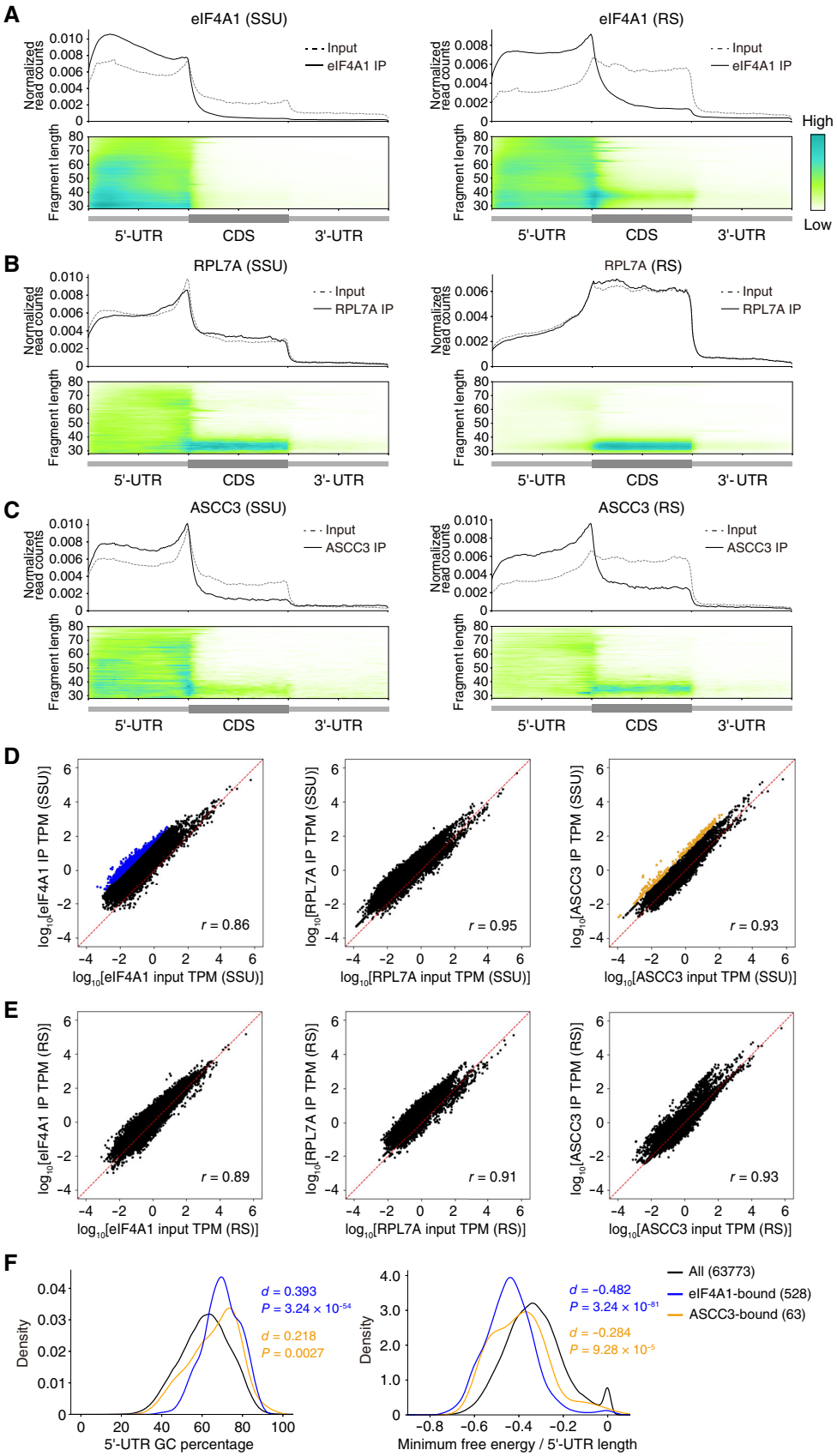

Figure 3.

Figure 3. Sel-TCP-seq analysis of eIF4A1-FLAG, RPL7A-HA, and ASCC3-FLAG in HEK293T cells.

A–C Metagene plots for full-length footprints prepared from the SSU (left) and RS (right) fractions of eIF4A1-FLAG KI (A), RPL7A-HA KI (B), and ASCC3-FLAG KI (C) HEK293T cells. The top plots show the results for Sel-TCP-seq and input, whereas the bottom plots show the results for only Sel-TCP-seq. Representative data from two replicates are shown. All reads were mapped to all human protein-coding transcripts with a 5′-UTR and 3′-UTR of > 100 nt (n = 37,916).

D, E Correlation of footprint TPM values for the SSU (D) and RS (E) fractions of eIF4A1-FLAG (left), RPL7A-HA (middle), and ASCC3-FLAG (right) with those for the corresponding input. For the SSU fractions, transcripts enriched > 50-fold in eIF4A1 IP or > 10-fold in ASCC3 IP compared with the corresponding input are shown in blue and orange, respectively. All human protein-coding transcripts with a coefficient of variation of > 0.5 in two technical replicates were plotted. Pearson's correlation coefficient (r) is indicated.

F Histograms for percentage GC content of the 5′-UTR (left) and for MFE of the 5′-UTR normalized by 5′-UTR length (right) for the indicated numbers of eIF4A1-bound, ASCC3-bound, and all transcripts. The effect size from Cliff's delta (d) and P-values (Mann–Whitney U test) for the transcripts are indicated.

were correlated with those of the corresponding inputs (Figs 3D and E, and EV1C and D). Transcripts that were enriched relative to the corresponding input (abscissa) by a factor of > 10 for ASCC3 immunoprecipitates or of > 50 for eIF4A1 immunoprecipitates (ordinate) were defined as transcripts that bind strongly to ASCC3 or eIF4A1, respectively (Fig 3D). The 5′-UTR of both of these sets of transcripts tended to have a higher percentage GC content and lower minimum free energy (MFE) relative to total transcripts (Fig 3F), suggesting that both eIF4A1 and ASCC3 preferentially bind to transcripts with rigid secondary structures in the 5′-UTR.

Loss of ASCC3 affects both scanning and translation

To explore the role of ASCC in translation, we transfected HEK293T cells with small interfering RNAs (siRNAs) targeting eIF4A1 and eIF4A2 (eIF4A1/A2 double knockdown (dKD)) or ASCC3 (ASCC3 KD). Each KD experiment was performed with two independent siRNAs (#1 and #2). Such transfection for 48 h resulted in a significant reduction in the corresponding abundance of eIF4A1, eIF4A2, or ASCC3 mRNAs and proteins (Fig 4A and B, Dataset EV4). eIF4A3 was not included in this analysis because it contributes to mRNA splicing, not to translation initiation (Chan *et al*, 2004). The amount of ASCC3 protein was upregulated in response to eIF4A1/A2 depletion (Fig 4A and B). The extent of eIF4A1 depletion at the protein level in eIF4A1/A2 dKD cells was relatively small compared with that at the mRNA level, suggestive of the operation of an unknown compensatory mechanism or a consequence of survival bias. It is also of note that the abundance of ASCC2 protein was reduced in cells depleted of ASCC3, suggesting that complex formation might stabilize the ASCC components.

To determine changes in global translation, we examined *O*-propargyl-puromycin (OPP) incorporation in the KD cells. We found that global translation was markedly decreased by the depletion of eIF4A, whereas it was slightly reduced or increased in ASCC3 KD #1 and #2 cells, respectively (Fig 4C), indicative of a negligible effect of ASCC3 loss on global translation. An integrated stress response was not induced in any of the KD cells, as assessed by immunoblot analysis of the phosphorylation of eIF2α as well as by determination of translation efficiency (see below) for the main open reading frame (ORF) of activating transcription factor 4 (ATF4; Fig EV2A and B). We performed Ribo-seq analysis with the KD cells and found that eIF4A1/A2 dKD and ASCC3 KD markedly affected translation efficiency (TE: Ribo-seq reads normalized by RNA-seq reads; Fig 4D, Dataset EV5). TE is a normalized value for each sample, which makes interpretation of results difficult if there are substantial differences in global translation between samples. Given the marked decrease in global translation induced by eIF4A depletion, an increased TE value might indicate slightly decreased translation, and a decreased TE value might represent a gene that is greatly affected by eIF4A depletion. However, given that ASCC3 loss showed little effect on global translation, the TE values in ASCC3 KD cells likely reflect true changes in translation. The percentage of Ribo-seq reads aligning with the 5′-UTR, CDS, or 3′-UTR did not appear to be altered in ASCC3 KD or eIF4A1/A2 dKD cells compared with control cells (Fig EV2C), indicating that translation of uORFs was not greatly affected by loss of ASCC3 or eIF4A. Given that ASCC3 was found to be associated with scanning ribosomes, we performed TCP-seq of the SSU fraction for eIF4A1/A2 dKD cells and ASCC3 KD cells to examine whether the loss of ASCC3 affects scanning ribosome occupancy (SRO: TCP-seq reads of the 5′-UTR normalized by RNA-seq reads; Dataset EV6). We found that SRO was also greatly perturbed in these cells (Fig 4E).

About 40% of transcripts with a reduced TE and 30% of those with a reduced SRO in ASCC3 KD cells also showed a decreased TE or SRO, respectively, in eIF4A1/A2 dKD cells (Fig EV2D and E). Furthermore, the correlation in SRO between ASCC3 KD and eIF4A1/A2 dKD was as high as that between the respective siRNAs #1 and #2 (Fig EV2F). These results indicated that eIF4A and ASCC3 regulate the scanning process for similar transcripts. We therefore performed TCP-seq analysis for the SSU fraction of triple-knockdown (tKD) cells lacking eIF4A1/eIF4A2 and ASCC3 (Fig EV2G) and found that the number of transcripts with a significantly altered SRO and the extent of the fold change in SRO were further increased in these cells compared with eIF4A1/A2 dKD cells (Fig EV2H and I), consistent with the finding of a compensatory increase in ASCC3 expression in response to eIF4A depletion.

ASCC3 depletion impairs PIC loading

Decreased PIC loading has been found to result in a reduction in the number of footprints throughout the 5′-UTR in TCP-seq analysis of the SSU fraction (Gupta *et al*, 2018; Sen *et al*, 2019). Metagene analysis of TCP-seq with transcripts for which SRO was reduced by eIF4A or ASCC3 depletion showed that the footprints in the 5′-UTR were substantially decreased in eIF4A1/A2 dKD and ASCC3 KD cells, suggestive of defective PIC loading (Figs 5A and EV3A). In contrast, metagene plots of transcripts with an increased SRO in eIF4A1/A2 dKD or ASCC3 KD cells showed a substantial increase in scanning ribosome footprints in the 5′-UTR (Figs 5B and EV3B). To examine whether such changes in SRO might affect TE, we evaluated the global association between changes in SRO and TE. We detected a mild correlation between TE and SRO for transcripts

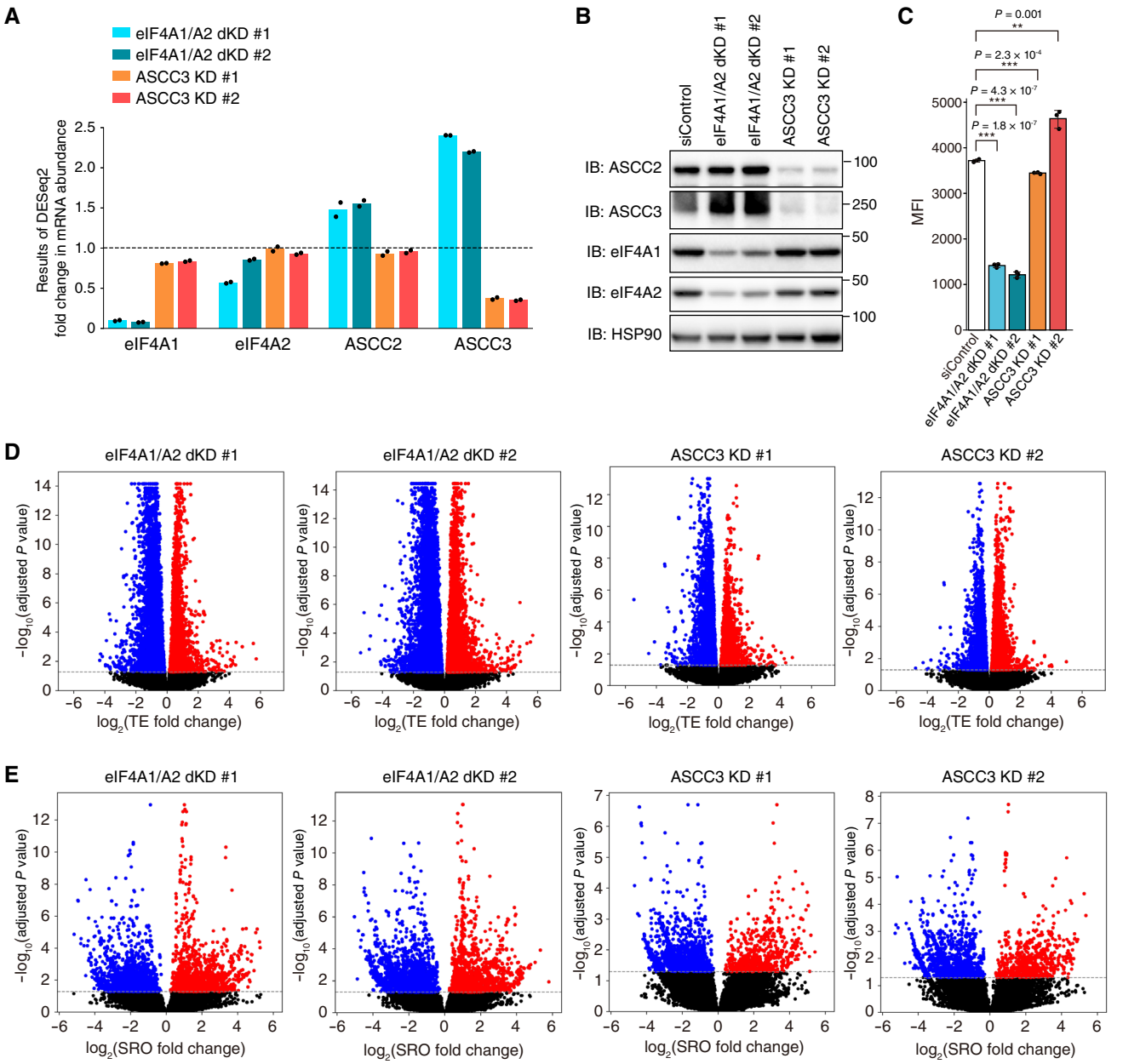

Figure 4. Altered TE and SRO in ASCC3-depleted cells.

A RNA-seq results for eIF4A1, eIF4A2, ASCC2, and ASCC3 in HEK293T cells transfected with siRNAs specific for eIF4A1 and eIF4A2 (eIF4A1/A2 dKD #1 or #2) or for ASCC3 (ASCC3 KD #1 or #2) relative to cells transfected with a control siRNA. The dashed line indicates a fold change of 1.

B Immunoblot analysis of the siRNA-transfected cells with the indicated antibodies.

C Quantitative analysis of global translation in the siRNA-transfected cells as monitored by OPP incorporation (n = 3 biologically independent samples). MFI, mean fluorescence intensity. Data are means ± s.d. $^{**}P < 0.01$, $^{***}P < 0.001$ (two-sided Student's t-test).

D, E Volcano plots for differential TE (D) and SRO (E). The changes in TE and SRO for eIF4A1/A2 dKD #1 and #2 and for ASCC3 KD #1 and #2 HEK293T cells compared with control cells were analyzed with RiboDiff. The gray dashed lines indicate an adjusted P-value of 0.05. P-values were calculated by chi-square test and adjusted by Benjamini–Hochberg method.

Source data are available online for this figure.

whose TE and SRO were significantly affected by the depletion of eIF4A or ASCC3 (Fig 5C). Furthermore, cumulative fraction analysis of transcripts with an increased or decreased SRO revealed a slight but significant increase or decrease in TE, respectively, for all eIF4A1/A2 dKD and ASCC3 KD cell lines (Fig 5D and E). These results suggested that changes in SRO induced by the loss of eIF4A or ASCC3 influence translational activity. A decrease in TE is likely attributable to decreased PIC loading, whereas an increase in TE may be due to the recruitment of excess PICs to transcripts that are less susceptible to the loss of eIF4A or ASCC3.

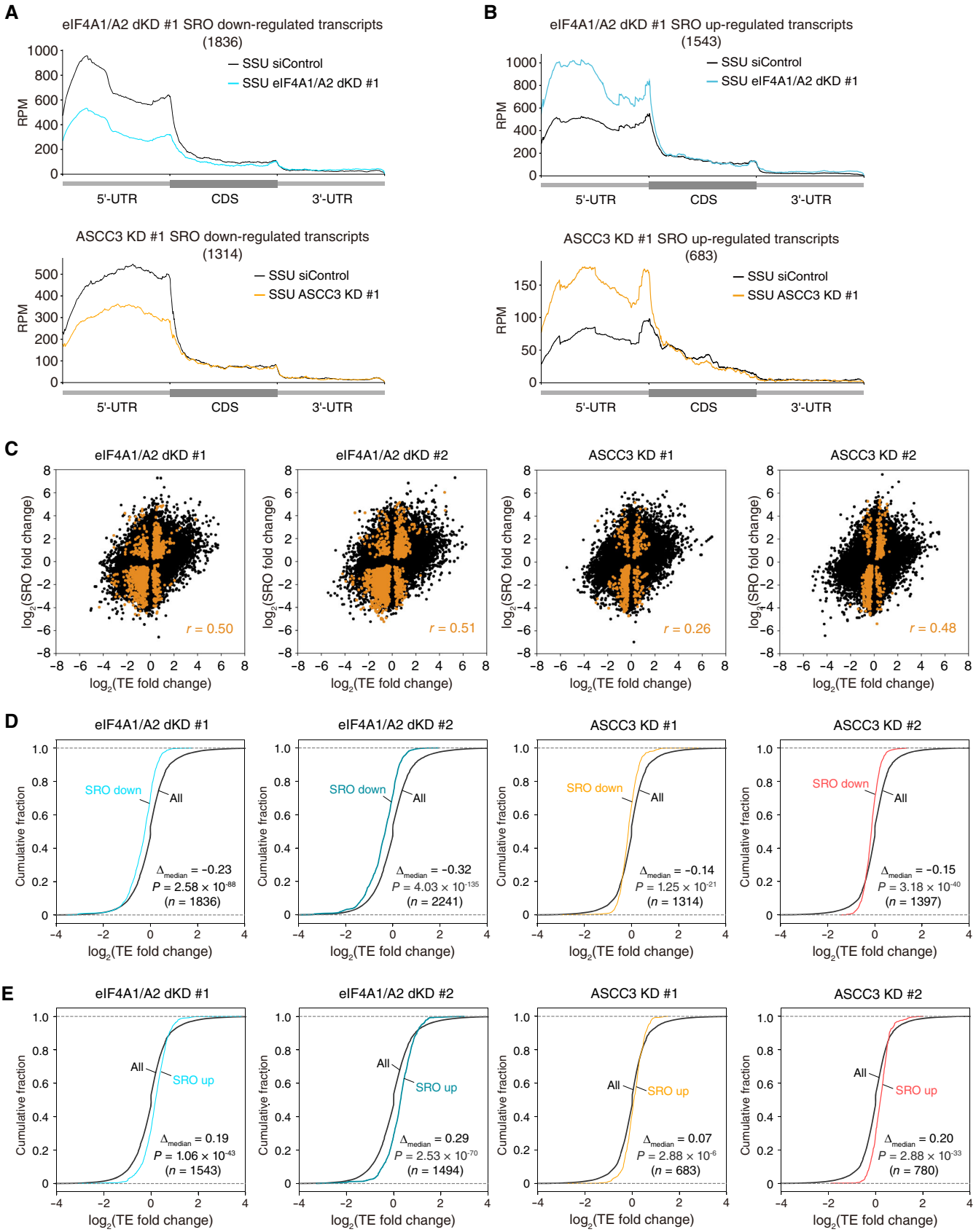

Figure 5.

Figure 5. Loss of ASCC3 reduces PIC loading.

A, B Metagene plots for full-length footprints obtained by TCP-seq analysis of the SSU fraction prepared from control, eIF4A1/A2 dKD #1, and ASCC3 KD #1 cells. Only transcripts for which SRO was significantly decreased (A) or increased (B) in eIF4A1/A2 dKD #1 or ASCC3 KD #1 cells compared with control cells were analyzed. RPM, reads per million mapped reads.

C Correlation of fold change in SRO with that in TE for eIF4A1/A2 dKD or ASCC3 KD cells relative to control cells. Orange dots indicate transcripts with significant changes in both TE and SE, with Pearson's correlation coefficient (r) for these transcripts being indicated.

D, E Cumulative fraction for fold change in TE in eIF4A1/A2 dKD or ASCC3 KD cells relative to control cells. Results are shown for all coding transcripts and for transcripts with a decreased (D) or increased (E) SRO. The P-values were calculated with the Mann–Whitney U test.

Analysis of transcripts with an altered TE in ASCC3-depleted cells

Metagene analysis of TCP-seq data was also performed for transcripts with an increased or decreased TE in eIF4A1/A2 dKD or ASCC3 KD cells, but no consistent trend was observed (Fig EV3C and D). We next analyzed total length, 5′-UTR length, percentage GC content, and MFE for transcripts with an increased or decreased TE in eIF4A1/A2 dKD or ASCC3 KD cells (Fig EV4A). The 5′-UTR of transcripts with a decreased TE in eIF4A1/A2 dKD cells tended to have a higher percentage GC content and a lower MFE, but this was not the case for ASCC3 KD cells (the effect size from Cliff's delta (d) was negligibly small, $|d| < 0.147$), which suggests that transcripts with rigid secondary structures in the 5′-UTR show a decreased TE in response to eIF4A loss. Although the length of the 5′-UTR did not differ, the full length of transcripts was longer for those with a decreased TE in eIF4A1/A2 dKD or ASCC3 KD cells. In addition, a higher percentage GC content and lower MFE were apparent for transcripts with an increased TE in ASCC3 KD cells, but the reason for these findings is not clear.

Of note, transcripts with a reduced TE in ASCC3 KD cells showed enrichment for lysine and asparagine codons in the CDS (Fig EV4B). Given that ribosome stalling occurs for proteins with polylysine tracts (Bengtson & Joazeiro, 2010; Brandman *et al*, 2012; Joazeiro, 2019; Ikeuchi *et al*, 2019a), the decreased TE of some transcripts in ASCC3 KD cells was likely attributable to defective dissociation of colliding ribosomes, which may account for the lack of a difference in percentage GC content or MFE for the 5′-UTR of transcripts with a decreased TE in ASCC3 KD cells. These results suggest that the two functions of ASCC in ribosome scanning and dissociation of colliding ribosomes independently affect translation and that the observed effects of ASCC3 KD may reflect the sum of the effects of the loss of these two separate functions.

ASCC is required for scanning ribosomes under certain conditions

A reduced speed of ribosomal scanning has been shown to result in the accumulation of SSU footprints near the transcription start site (TSS) compared with at the translation initiation site (TIS; *Sen et al*, 2019). We therefore analyzed the SSU footprint skew score to evaluate comprehensively a potential reduction in scanning speed (Fig 6A; Calviello *et al*, 2021). SSU footprint reads from the TSS to TIS (5′-UTR FP) were normalized by SSU footprint reads at −30 to +30 nucleotides (nt) relative to the TIS (TIS FP), and the ratio of KD to control for the values was defined as the SSU footprint skew score (Fig 6A, Dataset EV7). If KD of a factor of interest results in the accumulation of SSU footprints near the TSS rather than near the AUG initiation codon, the SSU footprint skew score becomes higher. Transcripts with an SSU footprint skew score of ≥ 2 were classified as skewed transcripts (Fig 6B). Kurtosis is an index of the sharpness of a frequency distribution; distributions with a greater kurtosis have sharper peaks and longer tails compared with the normal distribution. For eIF4A1/A2 dKD and ASCC3 KD cells, kurtosis of the SSU footprint skew score was 2–3 (that of the normal distribution is 0; Fig EV5A), indicating that the selected transcripts were affected by ASCC3 KD to the same extent as by eIF4A1/A2 dKD. Approximately 16% of the skewed transcripts in ASCC3 KD cells overlapped with those in eIF4A1/A2 dKD cells (Fig EV5B), suggesting that ASCC3 and eIF4A contribute to the regulation of scanning speed for similar sets of transcripts. The skewed transcripts tended to overlap with transcripts with an increased SRO, consistent with the accumulation of footprints near the TSS of the 5′-UTR in the skewed transcripts, but most skewed transcripts showed no significant change in SRO (Fig EV5C). These results indicate that there are three groups of transcripts with increased or decreased SRO and skewed transcripts, most of which are composed of different transcripts.

Metagene analysis of TCP-seq of the SSU fraction with the skewed transcripts resulting from eIF4A or ASCC3 depletion verified an accumulation of footprints near the TSS compared with near the AUG initiation codon in eIF4A1/A2 dKD and ASCC3 KD cells (Fig 6C). Cumulative fraction analysis of skewed transcripts resulting from eIF4A depletion showed a decrease in TE, whereas those resulting from ASCC3 depletion failed to show a significant change in TE (Fig 6D). We therefore examined the individual transcripts and found that TE was significantly reduced for a subset of skewed transcripts resulting from ASCC3 depletion (Fig 6E). These results suggested that ASCC3 deficiency slows the speed of scanning ribosomes, resulting in reduced translation in a substantial proportion, but not all, of the skewed transcripts.

5′-UTR–dependent regulation by ASCC3

Given that ASCC also contributes to the disassembly of collided 80S ribosomes, we performed luciferase assays with constructs containing only the 5′-UTR of transcripts affected by the loss of ASCC3 in order to exclude an effect on the CDS region. *RADX* mRNA showed a reduced TE and reduced number of SSU footprints throughout the 5′-UTR in ASCC3 KD cells (Fig 7A), suggestive of reduced PIC loading. The *DNAJB6* transcript also showed a reduced TE as well as an increase in the number of SSU footprints near the TSS but a decrease in that of those near the AUG initiation codon in ASCC3 KD cells (Fig 7A), suggestive of a reduced speed of scanning ribosomes. The *LDHA* transcript did not show a change in TE or SSU footprint pattern in ASCC3 KD cells compared with control cells (Fig 7A). We therefore constructed a reporter system by inserting the 5′-UTR sequence of *RADX*, *DNAJB6*, or *LDHA* transcripts

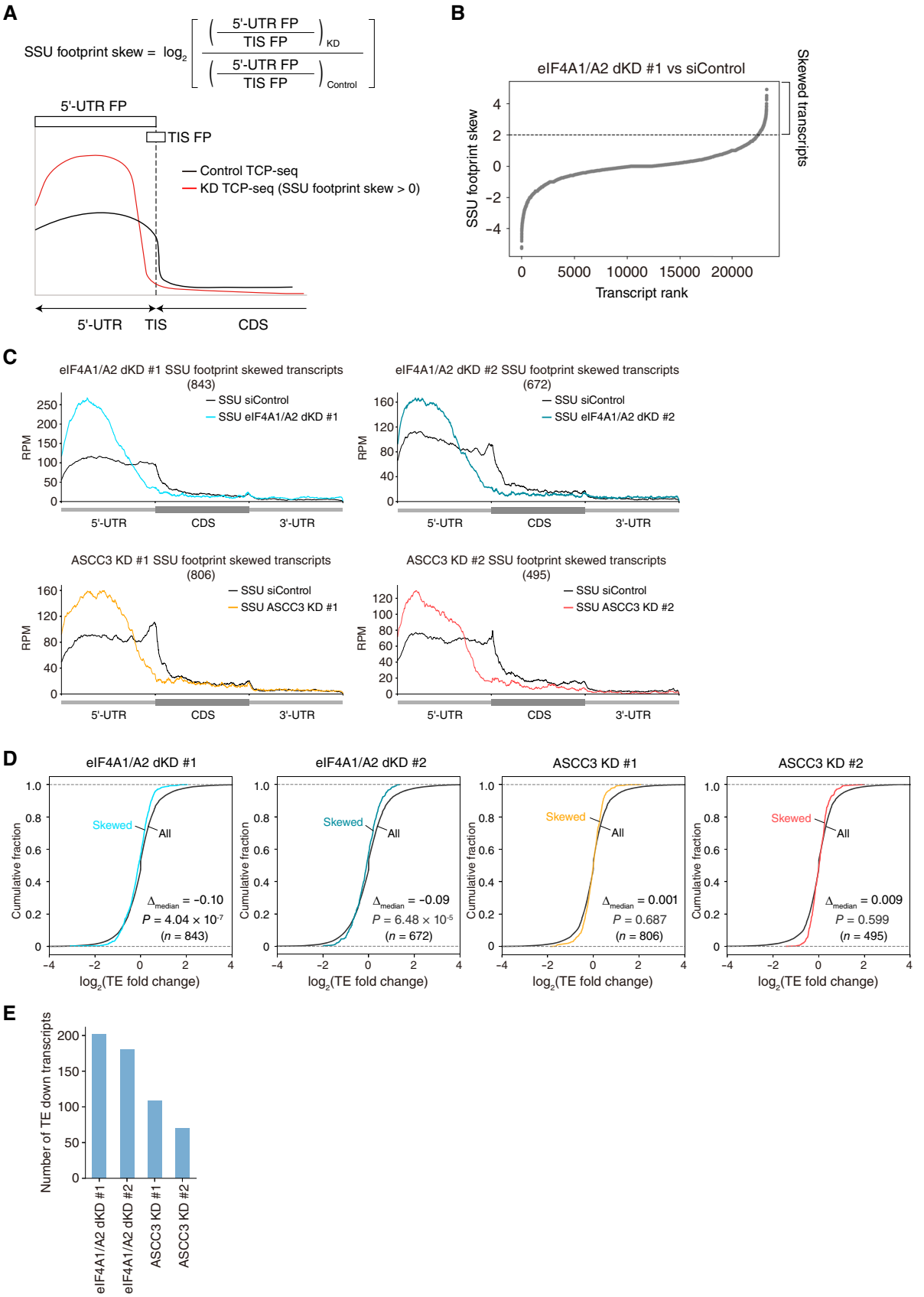

Figure 6.

Figure 6. Reduced speed of scanning ribosomes in cells depleted of ASCC3.

A Schematic representation and formula for calculation of the SSU footprint skew score. The regions corresponding to the 5′-UTR FP and TIS FP included in the calculation are indicated by white boxes.

B Plot of the SSU footprint skew score for eIF4A1/A2 dKD #1 cells versus control cells. The dashed line indicates a score of 2. Transcripts with a score of ≥2 were classified as skewed transcripts.

C Metagene plots for full-length footprints obtained by TCP-seq analysis of the SSU fraction prepared from control, eIF4A1/A2 dKD, and ASCC3 KD cells. Only skewed transcripts were analyzed.

D Cumulative fraction for fold change in TE in eIF4A1/A2 dKD or ASCC3 KD cells relative to control cells. Results are shown for all coding transcripts and skewed transcripts. The *P*-values were calculated with the Mann–Whitney *U* test.

E Number of transcripts showing significant downregulation of TE among skewed transcripts in eIF4A1/A2 dKD and ASCC3 KD cells.

Source data are available online for this figure.

upstream of the CDS for *Renilla* luciferase, which was linked to the CDS for firefly luciferase (internal control) by an internal ribosome entry site (IRES). Depletion of ASCC3 resulted in decreased translation of the *RADX* and *DNAJB6* constructs, but had no effect on translation of the *LDHA* construct (Fig 7B).

To determine the regions of the 5′-UTR that affect PIC loading or the speed of scanning ribosomes, we generated constructs lacking the first or second half of the 5′-UTR of *RADX* or *DNAJB6* transcripts (Fig 7C). The construct lacking the first half of the *RADX* 5′-UTR, but not that lacking the second half, failed to show reduced translation in response to ASCC3 depletion (Fig 7C), suggesting that the secondary structure of the mRNA near the TSS may suppress PIC loading. The construct lacking the first half of the *DNAJB6* 5′-UTR, but not that lacking the second half, also showed no effect of ASCC3 loss on translation (Fig 7C), suggesting that the accumulation of SSU footprints at ~30 to 50 nt from the TSS was attributable to a decreased speed of scanning ribosomes. For both *RADX* and *DNAJB6* transcripts, the MFE of the first half of the 5′-UTR was lower than that of the second half without a difference in percentage GC content (Fig 7D), suggesting that the secondary structure of the first half of each 5′-UTR is more stable than that of the second half. These results further suggested that ASCC3 regulates translation by modulating PIC loading and scanning ribosome speed in a manner dependent on the 5′-UTR sequence of specific transcripts.

Discussion

We have here performed Sel-TCP-MS to comprehensively identify the components of eIF4A1-bound scanning ribosomes, and we unexpectedly found that ASCC, which was previously shown to dissociate colliding 80S ribosomes, also associates with scanning ribosomes. Sel-TCP-seq of ASCC3 revealed that the protein is predominantly localized to the 5′-UTR of mRNAs. Furthermore, loss of ASCC3 resulted in a reduction in TE as a consequence of reduced PIC loading and a reduced speed of scanning ribosomes. These abnormalities were abrogated by the deletion of a portion of the 5′-UTR of affected transcripts. Although TCP-seq and luciferase reporter assays provide only indirect information regarding PIC loading and scanning dynamics, with biochemical analyses being needed to provide direct evidence, our results demonstrate that ASCC binds to scanning ribosomes and thereby regulates the translation initiation process.

We analyzed both our Sel-TCP-seq data as well as those from two previous studies (Bohlen *et al*, 2020; Wagner *et al*, 2020), and we found that the patterns around the start codon, such as the length of SSU fragments and the extent of their accumulation, differed among the three studies (Appendix Fig S2A). The accumulation of footprints was observed at −10 to −14 nt relative to the start codon in the data of Bohlen *et al* but at −1 to +4 nt in those of Wagner *et al* and in our data. These differences are likely attributable to differences in cell type or TCP-seq protocols. Bohlen *et al* performed their analysis with HeLa cells, whereas we and Wagner *et al* studied HEK293T cells. Bohlen *et al* fixed the cells with paraformaldehyde and dithiobis(succinimidyl propionate) and then treated them with RNase I at 4°C for 5 min, whereas we and Wagner *et al* fixed the cells with formaldehyde only and treated them with RNase I at 25°C or room temperature for 45 or 30 min, respectively.

Recent cryo-electron microscopy (cryo-EM) analysis has led to the proposal of an initial working model for the mechanism underlying splitting of the stalled leading ribosome by the yeast RQT complex (mammalian ASCC ortholog; Best *et al*, 2023). The yeast Slh1 helicase (mammalian ASCC3 helicase ortholog) comprises two cassettes (NH_2-terminal (NTC) and COOH-terminal (CTC) cassettes), each consisting of a RecA-like ATPase domain, a winged helix (WH) domain, and a Sec63-like domain. The RQT complex is located in close proximity to the mRNA entry channel and is stably docked to the 40S subunit of the stalled leading ribosome via the NTC of Slh1, with the CTC of Slh1 being positioned suitably for binding of the 3′ region of the mRNA. The CTC of Slh1 interacts with and pulls the 3′ region of the mRNA protruding from the leading ribosome, resulting in a conformational change of the latter. The trailing ribosome then serves as a wedge to promote dissociation of the 60S subunit of the leading ribosome.

However, it has been shown that there is only one scanning ribosome per mRNA in most human cells (Bohlen *et al*, 2020), with the result that scanning ribosomes are unlikely to collide on the 5′-UTR. In contrast, cryo-electron microscopy has detected RQT-bound 40S ribosomes after collided ribosomes have been released from the mRNA, suggesting that some of these released 40S ribosomes that are not deubiquitylated may be recruited to mRNA as an ASCC-bound PIC. It is therefore possible that, similar to the splitting of the stalled leading 80S ribosome, ASCC promotes translation initiation by binding to the eS10-polyubiquitylated PIC and scanning ribosome via the NTC of ASCC3 and to the 5′-UTR of the mRNA via the CTC of ASCC3.

We found that eIF4A and ASCC3 regulate similar transcripts and phenotypic exacerbation was observed in response to the loss of ASCC3 in combination with eIF4A depletion. Previous cryo-EM analysis has shown that eIF4A functions at a position near the mRNA exit channel of the 40S ribosome subunit (Querido *et al*, 2020), but a recent study has identified a second eIF4A that

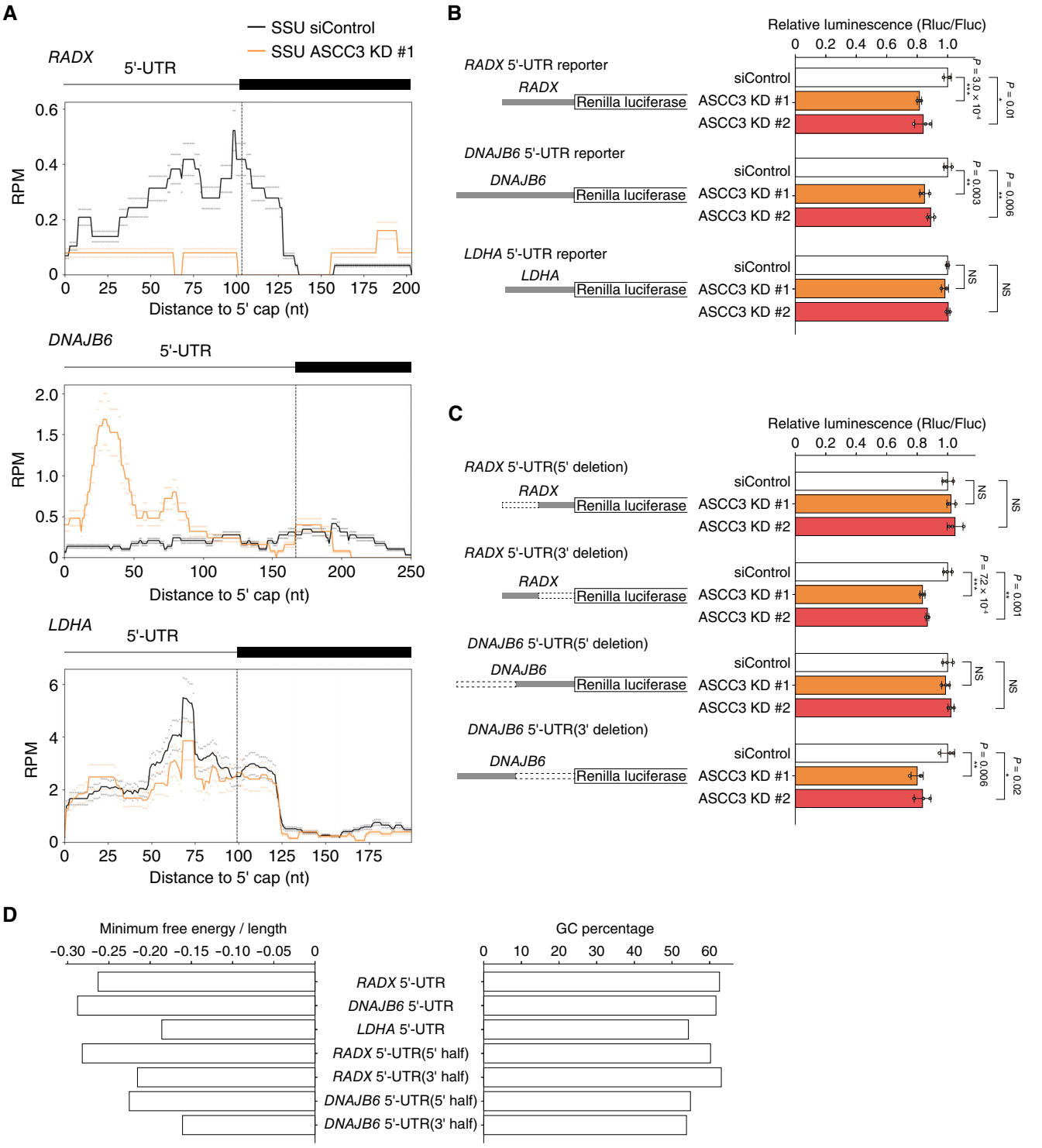

Figure 7. Dependence on the 5′-UTR for reduced translation of transcripts due to loss of ASCC3.

A Read aggregation plots of TCP-seq for *RADX*, *DNAJB6*, and *LDHA* mRNAs in the SSU fraction of control and ASCC3 KD #1 cells. The average of two replicates is shown.

B, C Luciferase assays for *RADX*, *DNAJB6*, and *LDHA* constructs (B) and for corresponding deletion mutants of the *RADX* and *DNAJB6* constructs (C) in control and ASCC3-depleted HEK293T cells. The results of the luciferase assays (right) and schematic representations of the constructs (left) are shown. The deleted regions of the *RADX* and *DNAJB6* constructs are indicated by dashed white boxes. Rluc, *Renilla* luciferase; Fluc, firefly luciferase. Assay data are means ± s.d. for three independent experiments. *$P < 0.05$, **$P < 0.01$, ***$P < 0.001$, NS (two-sided Student's *t*-test).

D MFE normalized by length (left) and percentage GC content (right) for the entire or 5′ or 3′ halves of the 5′-UTR for the indicated transcripts.

Source data are available online for this figure.

binds to the mRNA entry channel, in addition to the one that is part of eIF4F, which likely functions to unwind the secondary structure of mRNAs that enter the mRNA entry channel during scanning (preprint: Querido *et al*, 2022). The low helicase activity of eIF4A compared with many other helicases suggested that additional helicases may be required to scan the 5′-UTR of mRNAs with highly stable secondary structures, and ASCC3 may be one of them for a subset of transcripts. Although further detailed exploration of the proposed hypotheses is warranted, our results suggest that ASCC contributes not only to the dissociation of colliding 80S ribosomes but also to translation initiation.

Materials and Methods

Cells and culture conditions

HEK293T cells were obtained from American Type Culture Collection and were checked for mycoplasma contamination with the use of MycoAlert (Lonza). The cells were cultured under an atmosphere of 5% CO_2 at 37°C in Dulbecco's modified Eagle's medium supplemented with 10% fetal bovine serum (Life Technologies) and antibiotics.

Antibodies

Primary antibodies included those targeted to the following: eIF4A (Cell Signaling Technology, 2013), eIF4A1 (Thermo Fisher Scientific, 711505), eIF4A2 (Abcam, ab31218), eIF4E (Cell Signaling Technology, 2067), eIF4G (Cell Signaling Technology, 2469), eIF3B (Thermo Fisher Scientific, PA5-23278), eIF3D (Bethyl Laboratories, A301-758A), eIF2α (Cell Signaling Technology, 5324S), Ser^{51}-phosphorylated eIF2α (Cell Signaling Technology, 3398S), ASCC1 (Bethyl Laboratories, A303-871A), ASCC2 (Bethyl Laboratories, A304-020A), ASCC3 (Proteintech, 17627-1-AP), HSP90 (BD Biosciences, 610419), the V5 epitope (Thermo Fisher Scientific, R960CUS), the HA epitope (Abcam, ab9110), and the FLAG epitope (Merck, F1804). Normal mouse immunoglobulin G was obtained from Santa Cruz Biotechnology (K1017).

Generation of KI cells for epitope-tagged eIF4A1, ASCC3, and RPL7A

Sense and antisense oligonucleotides (Appendix Table S2) encoding single-guide RNAs (sgRNAs) were cloned into pX330 (Addgene). Targeting constructs for homologous recombination were cloned in pBluescript II SK (Stratagene) with the use of a NEBuilder HiFi DNA Assembly Master Mix Kit (New England Biolabs). HEK293T cells were transfected for 24 h with targeting vectors and pX330 encoding sgRNAs and were then subjected to selection in medium containing puromycin for 2 weeks before establishment of clonal cell lines by limiting dilution. eIF3D-V5/eIF4E-FLAG dKI cells were established previously (Ichihara *et al*, 2021).

RNA interference

HEK293T cells were transfected with 10 nM siRNAs with the use of Lipofectamine RNAiMAX (Invitrogen). Silencer Select Pre-Designed siRNAs (Thermo Fisher Scientific)—including negative control no. 1 (4390843), sieIF4A1 no. 1 (s4567), sieIF4A1 no. 2 (s4569), sieIF4A2 no. 1 (s4570), sieIF4A2 no. 2 (s4571), siASCC3 no. 1 (s21604), and siASCC3 no. 2 (s21605)—were used.

Lentivirus expression system

Human eIF4A1 and ASCC3 cDNAs were cloned separately into the pLVSIN-CMV Pur Vector (TaKaRa), and the resulting constructs were introduced along with pCMV-VSV-G (Addgene), pMDLg/pRRE (Addgene), and pRSV-Rev (Addgene) into HEK293T cells with the use of the X-tremeGENE 9 reagent (Roche). Culture supernatants containing recombinant lentiviruses were collected for infection of HEK293T cells for 24 h in the presence of polybrene (2 μg/ml). The cells were then subjected to selection by incubation for an additional 24 h in medium containing puromycin (2.5 μg/ml) and were cultured without puromycin for 48 h before experiments.

Measurement of protein synthesis

Global translation was monitored with the use of a PURO-Fluor Protein Synthesis Labeling Kit (Cayman Chemical). In brief, cells were incubated with OP-puro working solution for 30 min in a CO_2 incubator, collected, fixed with cell-based assay fixative for 5 min at room temperature, and washed twice with cell-based assay wash buffer. The cells were then incubated with 5 FAM-azide staining solution for 5 min at room temperature and washed twice with cell-based assay wash buffer before flow cytometric analysis with a FACSVerse instrument (BD).

Luciferase assays

DNA sequences encoding the 5′-UTR of human *LDHA*, *RADX*, and *DNAJB6* transcripts as well as corresponding deletion mutants were cloned into the pcDNA3 RLUC POLIRES FLUC vector (Addgene), and the resulting constructs were introduced into HEK293T cells with the use of the X-tremeGENE 9 reagent (Roche). Luciferase assays were performed with the use of a Dual-Luciferase Reporter Assay System (Promega) and Lumat LB 9510 Tube Luminometer (Berthold Technologies).

Ribo-seq

HEK293T cells were seeded at a density of 2.0×10^6 per 10-cm dish and subjected to the following analysis 48 h after siRNA transfection. The culture medium was removed, and the cells were immediately placed on ice, washed once with ice-cold phosphate-buffered saline (PBS), and lysed with a lysis buffer (50 mM Tris–HCl at pH 7.5, 150 mM NaCl, 5 mM $MgCl_2$, 1 mM dithiothreitol, 1% Triton X-100, and cOmplete EDTA-free protease inhibitor cocktail (Roche)) supplemented with cycloheximide (100 μg/ml). The lysates were incubated on ice for 10 min with TURBO DNase (Thermo Fisher Scientific) and then centrifuged at 20,380 *g* for 10 min at 4°C, and the resulting supernatants were collected, assayed for RNA concentration with a Qubit RNA BR Assay Kit (Thermo Fisher Scientific), incubated with RNase I (20 U per 10 μg of RNA, Epicentre) for 45 min at 25°C, and placed on ice before the addition of SUPERase•In RNase inhibitor (Invitrogen). The samples were then loaded

on a 1 M sucrose cushion (containing 20 mM Tris–HCl at pH 7.5, 150 mM NaCl, 5 mM $MgCl_2$, SUPERase•In at 10 U/ml, 1 mM dithiothreitol, and cycloheximide at 100 μg/ml), and the gradients were centrifuged at 100,000 rpm (417,200 *g*) for 1 h at 4°C in a Beckman TLA110 rotor. The resulting pellets were suspended in ribosome splitting buffer (20 mM Tris–HCl at pH 7.5, 300 mM NaCl, 5 mM EDTA, SUPERase•In at 20 U/ml, 1 mM dithiothreitol, and 1% Triton X-100) and subjected to purification with the use of an Amicon Ultra filtration device (100-kDa cutoff, Millipore) to deplete rRNAs. The purified RNA was subjected to selection on the basis of a size range of 17 to 34 nt by electrophoresis through a 15% polyacrylamide and Tris-borate-EDTA (TBE)–urea gel (SuperSep RNA, Fujifilm). The footprint fragments were treated with T4 polynucleotide kinase (New England Biolabs) to repair the 2′-3′ cyclic phosphates, a DNA linker including barcode sequences (NI-810 to NI-817; Appendix Table S2) was ligated with the use of T4 RNA ligase 2 and truncated K227Q (New England Biolabs), and the resulting products were purified on a 15% polyacrylamide and TBE-urea gel. Ribosomal RNAs were further depleted with the use of RiboZero Gold (Illumina). Reverse transcription (RT) was performed with the NI-802 primer (Appendix Table S2), and the resulting products were purified on a 15% polyacrylamide and TBE-urea gel. The purified cDNAs were circularized with circLigase II (Lucigen), and index sequences were then added by amplification with the polymerase chain reaction (PCR) as performed with the common primer (NI-798) and primers including index sequences (NI-799 and NI-822 to NI-826; Appendix Table S2). Products of the desired size were purified on a 15% polyacrylamide nondenaturing gel (SuperSep DNA, Fujifilm), and the libraries were sequenced with a NovaSeq 6000 system (Illumina).

RNA-seq

Total RNA was extracted from cell lysates with the use of a PureLink RNA Mini Kit (Thermo Fisher Scientific), and the quality of the purified RNA was assessed with a 2100 Bioanalyzer (Agilent). After mRNA selection with the use of a NEBNext Poly(A) mRNA Magnetic Isolation Module (New England Biolabs), libraries were prepared with the use of a NEBNext Ultra Directional RNA Library Prep Kit for Illumina (New England Biolabs). The cDNAs were sequenced with a NovaSeq 6000 system (Illumina).

Sample preparation for Sel-TCP analyses

Cells were seeded at a density of 8.0×10^6 cells per 15-cm dish, with 8 to 18 dishes per assay, and were cultured for 2 days. The subconfluent cells were treated for 10 min at room temperature with PBS containing 0.25% formalin, after which glycine was added to a final concentration of 125 mM and the cells were collected. The cells were washed three times with ice-cold PBS, lysed in a lysis buffer (50 mM Tris–HCl at pH 7.5, 150 mM NaCl, 5 mM $MgCl_2$, 1 mM dithiothreitol, 1% Triton X-100, and cOmplete EDTA-free protease inhibitor cocktail (Roche)) supplemented with cycloheximide (100 μg/ml), and incubated for 10 min on ice. The lysates were centrifuged at 20,380 *g* for 10 min at 4°C, and the resulting supernatants were collected, assayed for RNA concentration with a Qubit RNA BR Assay Kit (Thermo Fisher Scientific), incubated with RNase I (20 U per 10 μg of RNA, Thermo Fisher Scientific) at 25°C for 45 min, and then placed on ice before the addition of SUPERase•In RNase inhibitor (Invitrogen). The samples were loaded on a 5% to 30% sucrose gradient (containing 20 mM Tris–HCl at pH 7.5, 150 mM NaCl, 5 mM $MgCl_2$, 1 mM dithiothreitol, cycloheximide at 100 μg/ml, and SUPERase•In at 10 U/ml) and centrifuged at 38,200 rpm (180,000 *g*) for 4 h at 4°C in a Himac P40ST rotor. The gradient was fractionated with the use of a TRIAX gradient-profiling system and AC-5700P microcollector. Polysome profiles were determined by measurement of absorbance at 260 nm. Dynabeads Protein G (Veritas) was conjugated with antibodies to FLAG, to HA, or to V5 by incubation overnight at 4°C in lysis buffer supplemented with 0.5% bovine serum albumin, and they were washed three times with lysis buffer before use. Small portions of the SSU or RS fractions were stored for input or TCP-seq, and the remaining samples were incubated with the beads for 90 min at 4°C. The resulting immunoprecipitates were washed four times with a wash buffer (50 mM Tris–HCl at pH 7.5, 300 mM NaCl, 1 mM dithiothreitol, and 0.1% Triton X-100). For Sel-TCP-seq analysis, 250 μl of decrosslinking buffer (1% SDS, 10 mM EDTA, 10 mM Tris–HCl at pH 7.5, and 10 mM glycine), 750 μl of ISOGEN LS (Nippon Gene), and 200 μl of chloroform were added to the beads, which were then incubated for 45 min at 65°C before purification of RNA by precipitation with isopropanol. For LC–MS/MS and immunoblot analyses, purified proteins were eluted either by direct incubation of the beads with SDS sample buffer for 45 min at 95°C, by incubation of the beads first for 10 min at room temperature with 20 μl of FLAG peptide (Sigma-Aldrich) at 0.5 mg/ml and then for 45 min at 95°C in SDS sample buffer, or by incubation of the beads for 30 min at room temperature with 20 μl of HA peptide (MBL Life Science) at 0.5 mg/ml and then for 45 min at 95°C in SDS sample buffer. The purified proteins and RNAs were then applied to LC–MS/MS, immunoblot, or Sel-TCP-seq analysis as described below.

LC–MS/MS analysis

Purified proteins were fractionated by SDS-polyacrylamide gel electrophoresis on a 10% gel and subjected to silver staining. Protein bands were excised from the gel and subjected to in-gel digestion, and the resulting peptides were dissolved in a solution comprising 0.1% trifluoroacetic acid and 2% acetonitrile for analysis with an LTQ Orbitrap Velos Pro mass spectrometer (Thermo Fisher Scientific) coupled with a nanoLC instrument (Advance, Michrom BioResources) and HTC-PAL autosampler (CTC Analytics). Peptide separation was performed with an in-house–pulled fused silica capillary (internal diameter of 0.1 mm and length of 15 cm, Nikkyo Technos) packed with 3-μm C18 L-column (Chemicals Evaluation and Research Institute, Japan). The mobile phases consisted of 0.1% formic acid (A) and 100% acetonitrile (B). Peptides were eluted with a gradient of 5% to 40% B for 30 min, 40% to 95% B for 1 min, and then 90% B for 9 min at a flow rate of 200 nl/min. Collision-induced dissociation (CID) spectra were acquired automatically in the data-dependent scan mode with the dynamic exclusion option. Full MS spectra were obtained with Orbitrap in the mass/charge (m/z) range of 300 to 1,600 with a resolution of 60,000 at m/z 400. The 12 most intense precursor ions for the full MS spectra were selected for subsequent ion-trap MS/MS analysis with the automated gain control (AGC) mode. The AGC was set to 1.00×10^4. The normalized collision energy values were set to

35%. Acquired MS data were analyzed with MaxQuant and the human UniProt KB database.

Immunoblot analysis

Samples were subjected to SDS-polyacrylamide gel electrophoresis on 5–20% ExtraPAGE One Precast Gels (Nacalai Tesque). Membranes were incubated consecutively with primary antibodies and horseradish peroxidase–conjugated secondary antibodies (Promega), and signals were visualized with SuperSignal West Pico PLUS (Thermo Fisher Scientific) reagents and with a ChemiDoc imaging system (Bio-Rad).

TCP-seq and Sel-TCP-seq

Purified RNA was selected according to size in the range of 17 to 100 nt by electrophoresis in a 15% polyacrylamide and TBE-urea gel and was then subjected to dephosphorylation, DNA linker ligation, and rRNA depletion with RiboZero Gold as described for the Ribo-seq protocol. RT was performed with the use of the SI-019 primer (Appendix Table S2), and the resulting products were purified on a 15% polyacrylamide and TBE-urea gel. The second linker (SI-018; Appendix Table S2) was ligated by incubation overnight at 25°C with T4 RNA Ligase 1 (ssRNA Ligase), High Concentration (New England Biolabs). The products were then amplified by PCR with the same primers as used for the Ribo-seq protocol, and those of the desired size were purified by electrophoresis through a 15% polyacrylamide nondenaturing gel. The libraries were sequenced with a NovaSeq 6000 system (Illumina).

Read processing and analysis

Adaptor sequences were trimmed from raw reads with the use of cutadapt. Reads of low quality were discarded with the use of fastq_quality_trimmer and fastq_quality_filter of the FASTX-Toolkit. Ribosomal RNA reads were removed by alignment with human rRNA sequences with the use of STAR, and the remaining reads were aligned with the human transcriptome (GRCh38.p13) and human genome (hg38) also with the use of STAR. Multiple mappings were allowed. Metagene analysis was performed with custom Python script and with the use of Numpy (v1.17.3) and Pysam (v0.15.3). The coverage of Sel-TCP-seq reads was calculated across the 5′-UTR, CDS, and 3′-UTR of transcripts. Heat maps of counts per fragment length were colored according to the sum of counts from all transcripts at a given position for a given fragment length. Reads of Sel-TCP-seq and input mapped to human coding transcripts were counted with the use of featureCounts, and transcripts per kilobase million (TPM) values were calculated. Minimum free energy (MFE) of RNA was calculated with the use of the Vienna RNA package.

Statistics and reproducibility

We used DESeq2 to analyze differential expression from RNA-seq reads (Love *et al*, 2014) and the generalized linear model in RiboDiff to analyze differential TE and differential SRO (Zhong *et al*, 2017). Pearson's correlation was calculated in Python 3.6.8 with the use of Pandas (v0.25.3). Effect size was calculated with Cliff's delta. The two-sided Student's *t*-test, Welch's *t*-test, and Mann–Whitney *U* test were performed in Python 3.6.8 with the use of Scipy (v1.2.1). For extraction of differentially expressed genes, we used an adjusted *P*-value (false discovery rate (FDR) q value) of < 0.05. A *P*-value of < 0.05 was otherwise considered statistically significant. All experiments were performed at least twice with similar results.

Data availability

The datasets produced in this study are available in the following databases:

- Sequencing data: Gene Expression Omnibus GSE186502 (https://www.ncbi.nlm.nih.gov/geo/query/acc.cgi?acc=GSE186502).
- Protein interaction IP-MS data: ProteomeXchange PXD029301, PXD029302, PXD029303 (http://proteomecentral.proteomexchange.org/cgi/GetDataset?ID=PXD029301; http://proteomecentral.proteomexchange.org/cgi/GetDatasetID=PXD029302; http://proteomecentral.proteomexchange.org/cgi/GetDatasetID=PXD029303).

Expanded View for this article is available online.

Acknowledgments
We thank L. Cui and Research Promotion Unit of Medical Institute of Bioregulation at Kyushu University for technical assistance as well as A. Ohta for help with preparation of the manuscript. Computations were performed in part on the NIG supercomputer at ROIS National Institute of Genetics. This research was supported in part by KAKENHI grants from Japan Society for the Promotion of Science (JSPS) and the Ministry of Education, Culture, Sports, Science, and Technology of Japan to AM (JP20H05928) and to KIN (JP18H05215), as well as by grants from Japan Agency for Medical Research and Development to AM (21gm6410018) and to KIN (21wm0425002).

Author contributions
Yuki Kito: Formal analysis; validation; investigation; visualization; writing – original draft. **Akinobu Matsumoto:** Conceptualization; resources; data curation; formal analysis; supervision; funding acquisition; validation; investigation; visualization; methodology; writing – original draft; project administration; writing – review and editing. **Kazuya Ichihara:** Data curation; software; formal analysis; validation; investigation; methodology; writing – original draft; writing – review and editing. **Chisa Shiraishi:** Formal analysis; methodology. **Ronghao Tang:** Formal analysis. **Atsushi Hatano:** Data curation; formal analysis; methodology. **Masaki Matsumoto:** Data curation; formal analysis; supervision. **Peixun Han:** Data curation; formal analysis. **Shintaro Iwasaki:** Data curation; formal analysis; supervision. **Keiichi I Nakayama:** Conceptualization; supervision; funding acquisition; writing – original draft; project administration; writing – review and editing.

Disclosure and competing interests statement
The authors declare that they have no conflict of interest.

References

Archer SK, Shirokikh NE, Beilharz TH, Preiss T (2016) Dynamics of ribosome scanning and recycling revealed by translation complex profiling. *Nature* 535: 570 – 574

Bengtson MH, Joazeiro CAP (2010) Role of a ribosome-associated E3 ubiquitin ligase in protein quality control. *Nature* 467: 470 – 473

Best K, Ikeuchi K, Kater L, Best D, Musial J, Matsuo Y, Berninghausen O, Becker T, Inada T, Beckmann R (2023) Structural basis for clearing of ribosome collisions by the RQT complex. *Nat Commun* 14: 921

Bohlen J, Fenzl K, Kramer G, Bukau B, Teleman AA (2020) Selective 40S footprinting reveals cap-tethered ribosome scanning in human cells. *Mol Cell* 79: 561 – 574

Bohlen J, Roiuk M, Neff M, Teleman AA (2023) PRRC2 proteins impact translation initiation by promoting leaky scanning. *Nucleic Acids Res* gkad135

Brandman O, Stewart-Ornstein J, Wong D, Larson A, Williams CC, Li GW, Zhou S, King D, Shen PS, Weibezahn J *et al* (2012) A ribosome-bound quality control complex triggers degradation of nascent peptides and signals translation stress. *Cell* 151: 1042 – 1054

Calviello L, Venkataramanan S, Rogowski KJ, Wyler E, Wilkins K, Tejura M, Thai B, Krol J, Filipowicz W, Landthaler M *et al* (2021) DDX3 depletion represses translation of mRNAs with complex 5′ UTRs. *Nucleic Acids Res* 49: 5336 – 5350

Chan CC, Dostie J, Diem MD, Feng WQ, Mann M, Rappsilber J, Dreyfuss G (2004) eIF4A3 is a novel component of the exon junction complex. *RNA* 10: 200 – 209

Gupta N, Lorsch JR, Hinnebusch AG (2018) Yeast Ded1 promotes 48S translation pre-initiation complex assembly in an mRNA-specific and eIF4F-dependent manner. *Elife* 7: e38892

Hashimoto S, Sugiyama T, Yamazaki R, Nobuta R, Inada T (2020) Identification of a novel trigger complex that facilitates ribosome-associated quality control in mammalian cells. *Sci Rep* 10: 3422

Hinnebusch AG (2017) Structural insights into the mechanism of scanning and start codon recognition in eukaryotic translation initiation. *Trends Biochem Sci* 42: 589 – 611

Ichihara K, Matsumoto A, Nishida H, Kito Y, Shimizu H, Shichino Y, Iwasaki S, Imami K, Ishihama Y, Nakayama KI (2021) Combinatorial analysis of translation dynamics reveals eIF2 dependence of translation initiation at near-cognate codons. *Nucleic Acids Res* 49: 7298 – 7317

Ikeuchi K, Izawa T, Inada T (2019a) Recent progress on the molecular mechanism of quality controls induced by ribosome stalling. *Front Genet* 9: 743

Ikeuchi K, Tesina P, Matsuo Y, Sugiyama T, Cheng J, Saeki Y, Tanaka K, Becker T, Beckmann R, Inada T (2019b) Collided ribosomes form a unique structural interface to induce Hel2-driven quality control pathways. *EMBO J* 38: e100276

Ingolia NT, Ghaemmaghami S, Newman JR, Weissman JS (2009) Genome-wide analysis *in vivo* of translation with nucleotide resolution using ribosome profiling. *Science* 324: 218 – 223

Jankowsky E (2011) RNA helicases at work: binding and rearranging. *Trends Biochem Sci* 36: 19 – 29

Joazeiro CAP (2019) Mechanisms and functions of ribosome-associated protein quality control. *Nat Rev Mol Cell Biol* 20: 368 – 383

Juszkiewicz S, Speldewinde SH, Wan L, Svejstrup JQ, Hegde RS (2020) The ASC-1 complex disassembles collided ribosomes. *Mol Cell* 79: 603 – 614

Kumar P, Hellen CUT, Pestova TV (2016) Toward the mechanism of eIF4F-mediated ribosomal attachment to mammalian capped mRNAs. *Genes Dev* 30: 1573 – 1588

Lapointe CP, Grosely R, Sokabe M, Alvarado C, Wang J, Montabana E, Villa N, Shin BS, Dever TE, Fraser CS *et al* (2022) eIF5B and eIF1A reorient initiator tRNA to allow ribosomal subunit joining. *Nature* 607: 185 – 190

LeFebvre AK, Korneeva NL, Trutschl M, Cvek U, Duzan RD, Bradley CA, Hershey JWB, Rhoads RE (2006) Translation initiation factor eIF4G-1 binds to eIF3 through the eIF3e subunit. *J Biol Chem* 281: 22917 – 22932

Love MI, Huber W, Anders S (2014) Moderated estimation of fold change and dispersion for RNA-seq data with DESeq2. *Genome Biol* 15: 550

Murat P, Marsico G, Herdy B, Ghanbarian A, Portella G, Balasubramanian S (2018) RNA G-quadruplexes at upstream open reading frames cause DHX36-and DHX9-dependent translation of human mRNAs. *Genome Biol* 19: 229

Querido JB, Sokabe M, Kraatz S, Gordiyenko Y, Skehel JM, Fraser CS, Ramakrishnan V (2020) Structure of a human 48S translational initiation complex. *Science* 369: 1220 – 1227

Querido JB, Sokabe M, Díaz-López I, Gordiyenko Y, Fraser CS, Ramakrishnan V (2022) The structure of a human translation initiation complex reveals two independent roles for the helicase eIF4A. *bioRxiv* https://doi.org/10.1101/2022.12.07.519490 [PREPRINT]

Sen ND, Gupta N, Archer SK, Preiss T, Lorsch JR, Hinnebusch AG (2019) Functional interplay between DEAD-box RNA helicases Ded1 and Dbp1 in preinitiation complex attachment and scanning on structured mRNAs *in vivo*. *Nucleic Acids Res* 47: 8785 – 8806

Shen L, Pelletier J (2020) General and target-specific DExD/H RNA helicases in eukaryotic translation initiation. *Int J Mol Sci* 21: 4402

Shirokikh NE, Preiss T (2018) Translation initiation by cap-dependent ribosome recruitment: recent insights and open questions. *WIREs RNA* 9: e1473

Shirokikh NE, Archer SK, Beilharz TH, Powell D, Preiss T (2017) Translation complex profile sequencing to study the *in vivo* dynamics of mRNA-ribosome interactions during translation initiation, elongation and termination. *Nat Protoc* 12: 697 – 731

Singleton MR, Dillingham MS, Wigley DB (2007) Structure and mechanism of helicases and nucleic acid translocases. *Annu Rev Biochem* 76: 23 – 50

Villa N, Do A, Hershey JWB, Fraser CS (2013) Human eukaryotic initiation factor 4G (eIF4G) protein binds to eIF3c, -d, and -e to promote mRNA recruitment to the ribosome. *J Biol Chem* 288: 32932 – 32940

Wagner S, Herrmannova A, Hronova V, Gunisova S, Sen ND, Hannan RD, Hinnebusch AG, Shirokikh NE, Preiss T, Valasek LS (2020) Selective translation complex profiling reveals staged initiation and co-translational assembly of initiation factor complexes. *Mol Cell* 79: 546 – 560

Zhong Y, Karaletsos T, Drewe P, Sreedharan VT, Kuo D, Singh K, Wendel HG, Ratsch G (2017) RiboDiff: detecting changes of mRNA translation efficiency from ribosome footprints. *Bioinformatics* 33: 139 – 141

